Title

I. A Study of Angle-resolved Photoemission Extended Fine Structure as Applied to the Ni 3p Core-level of a Clean Ni(111) Surface

Author

Huff, W.R.A.

Publication Date

1996-02-26

LBL-38423
UC-401
Preprint

Lawrence Berkeley Laboratory
UNIVERSITY OF CALIFORNIA

Accelerator & Fusion Research Division

Submitted to Physical Review B

I: A Study of Angle-Resolved Photoemission Extended Fine Structure as Applied to the Ni 3*p* Core-Level of a Clean Ni(111) Surface

W.R.A. Huff, Y. Chen, S.A. Kellar, E.J. Moler, Z. Hussain, Z.Q. Huang, and D.A. Shirley

February 1996

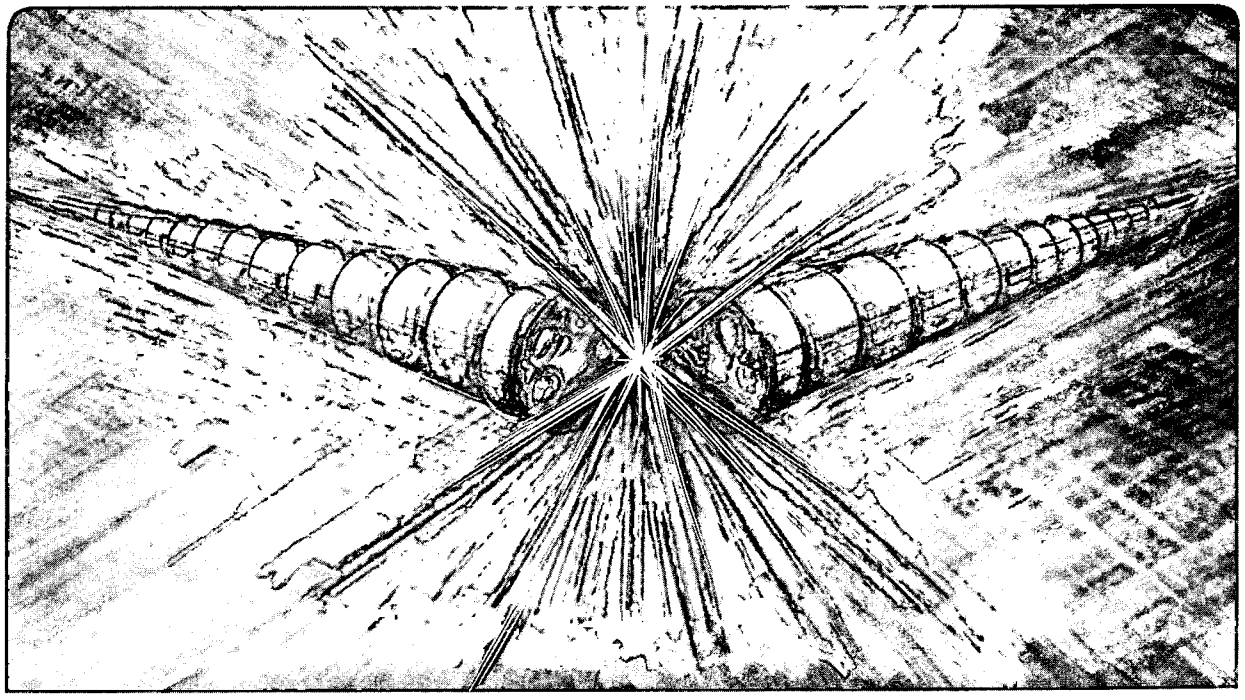

Prepared for the U.S. Department of Energy under Contract Number DE-AC03-76SF00098

DISCLAIMER

LBL-38423
LSBL-312
UC-401

I: A STUDY OF ANGLE-RESOLVED PHOTOEMISSION EXTENDED FINE STRUCTURE AS APPLIED TO THE NI 3*p* CORE-LEVEL OF A CLEAN Ni(111) SURFACE*

W.R.A. Huff[a,b], Y. Chen[c], S.A. Kellar[a,b], E.J. Moler[a,b], Z. Hussain[a], Z.Q. Huang[d], and D.A. Shirley[c]

[a]Advanced Light Source, Lawrence Berkeley National Laboratory, University of California, Berkeley, California 94720
[b]The University of California, Department of Chemistry, Berkeley, California 94720
[c]The Pennsylvania State University, Department of Chemistry and Physics, University Park, Pennsylvania 16802
[d]Present address: James Franck Inst., University of Chicago, IL 60637

*This work was supported by the Director, Office of Energy Research, Office of Basic Energy Sciences, Chemical Sciences Division, of the U.S. Department of Energy, under Contract No. DE-AC03-76SF00098.

I. A Study of Angle-Resolved Photoemission Extended Fine Structure as Applied to the Ni 3*p* Core-Level of a Clean Ni(111) Surface

W.R.A. Huff,[a,b] Y. Chen,[c] S.A. Kellar,[a,b] E.J. Moler,[a,b]
Z. Hussain,[a] Z.Q. Huang,[d] and D.A. Shirley[c]

[a]Lawrence Berkeley National Laboratory, Berkeley, CA 94720
[b]The University of California, Dept. of Chemistry, Berkeley, CA 94720
[c]The Pennsylvania State University, Dept. of Chemistry and Physics, University Park, PA 16802
[d]Present address: James Franck Inst., U. of Chicago, IL 60637

ABSTRACT

The first non-*s* initial state angle-resolved photoemission extended fine structure (ARPEFS) study of a clean surface for the purpose of further understanding the technique is reported. The sample was a Ni(111) single crystal and normal photoemission data were taken from the Ni 3*p* core levels. The spin-orbit splitting between the Ni $3p_{3/2}$ and Ni $3p_{1/2}$ core-levels was not well resolved and yet an oscillatory ARPEFS curve was obtained with frequencies corresponding to scattering path-length differences as shown by the Fourier transform (FT). The clean surface ARPEFS data resemble data for adsorbate systems, showing strong backscattering signals from atoms up to four layers below the source atoms. Also, the data show a peak in the FT corresponding to scattering from the six nearest neighbor atoms in the same crystal layer as the emitting atoms. This result has not been seen before because it is forbidden by symmetry for *s* initial state normal photoemission; however, it is expected for *p* initial state normal photoemission. Evidence was seen for single-scattering events from atoms laterally distant from the emitting atom as well as double-scattering events. Using a newly developed modeling code, the ARPEFS data were fit and the forward scattering and backscattering contributions were studied.

PACS Number: *61.14.-x, 61.14.Qp, 61.14.Rq, 68.35.Bs, 68.55.Jk*

I. INTRODUCTION

Angle-resolved photoemission extended fine-structure (ARPEFS) is a proved technique for determining surface structures.[1-5] ARPEFS has been used to determine the structures of metal and non-metal atomic adsorbate systems as well as molecular adsorbates on conducting single crystal surfaces. ARPEFS yields accurate information about both the local structure around the adsorbates and the adsorbate-induced relaxation of the substrates.[6-12] These studies have shown that ARPEFS data from adsorbate/substrate systems, along with the Fourier transforms (FTs) of the data, can be described in terms of backscattering events. The positions of all the strong peaks in ARPEFS-FTs from adsorbed surfaces can be predicted from a trial structure with fairly good accuracy based on a single-scattering cluster (SSC) model together with the concept of a backscattering cone.

The purpose here is to explore the applicability of ARPEFS to non-*s* initial state photoemission of clean surfaces. The immediate goal is to observe and to understand the phenomenon in a simple, known system. The long-range goal is to develop a method for studying photoemission from an arbitrary initial state as well as to determine the atomic structure of interfaces, for which ARPEFS seems ideally suited. In favorable cases, atomic relaxation and reconstruction could be studied as well. In such studies, the elemental and chemical specificity of ARPEFS and its sensitivity to atomic layers that are several layers below the surface would confer certain advantages.

In using ARPEFS to study clean surfaces, the photoelectron signals from surface and bulk atoms will in some cases be resolvable, either directly or through fitting procedures. In these cases, the data analysis would be

based on two ARPEFS curves. For the more common case in which signals from different layers cannot be resolved, reconstruction or relaxation effects may still be modeled by fitting the single experimental ARPEFS curve. Due to the strength of the bulk signal, this curve may not be surface sensitive enough to yield a conclusion about possible surface reconstruction.

Most of the previous ARPEFS studies have been based on photoemission data from atomic *s* core-level initial states, for which the selection rules $\Delta\ell_i = \pm 1$, and $\Delta m_i = 0$ give a p_o-wave final state. Experience with ARPEFS data from non-*s* initial states and their FTs is very limited, however.[13-15] For non-*s* initial states ($\ell_i \neq 0$), the photoelectron final state is made up of partial waves with orbital quantum numbers $\ell_i + 1$ and $\ell_i - 1$, and a phase relationship between them which leads to interference between the partial waves. Note that the allowed *m* levels will be populated in the final state. Thus, with a *p* initial state, the partial waves consist of $\ell_f = 0$, $m_f = m_i = 0$ as well as $\ell_f = 2$, $m_f = m_i = 0, \pm 1$. The partial wave radial dipole matrix elements and the phase shifts are generally energy dependent. Despite these complications, there are a number of interesting experimental situations for which ARPEFS studies on a non-*s* initial state may be the only practical method of study.

The data presented here are photoemission from a clean Ni(111) surface, for which the surface and bulk 3*p* core-level peaks are unresolved. In fact, the spin-orbit splitting between the Ni $3p_{3/2}$ and Ni $3p_{1/2}$ peaks was not well resolved and yet an oscillatory ARPEFS curve was obtained with frequencies corresponding to scattering path-length differences as shown by the FT. The ARPEFS data resemble data for adsorbate systems and show strong backscattering signals from atoms up to four layers *below* the source atoms.

A new result was obtained in the FT analysis of this p initial state ARPEFS curve. In addition to the backscattering, the data show a peak in the FT corresponding to scattering from the six nearest neighbor atoms in the same crystal layer as the emitting atoms. This result is forbidden by symmetry for s initial state normal photoemission scattering from a point potential, but it is expected from p initial state photoemission. Additionally, evidence was seen for single-scattering events from atoms laterally distant from the emitting atom as well as double-scattering events.

In modeling these data, it is expected that the electron mean free path calculation is important in obtaining a close fit to the data. It is not yet clear which calculation method for determining the mean free path is the most accurate. Certainly, many emitters lie several layers below the surface region and their signal never escapes the crystal. The mean free path was calculated using the exponential damping factor $e^{-r/\lambda}$. The typically used $\lambda = ck$ formula is compared to the newer TPP-2 formalism.[16-18]

Finally, an adsorbate system, $\sqrt{3}\times\sqrt{3}R30°$Cl/Ni(111),[19] is compared with this Ni $3p$ data. Although this previously published data was photoemission taken from the Cl $1s$ core level, the data from the s versus p initial states agree in that they are roughly 180° out of phase. Additionally, the FTs are similar and the backscattering cone model is supported by this work.

It is appropriate to note here that photoelectron holography signals from clean surfaces are dominated by forward scattering, with atomic positions being imaged up to three layers *ahead* of the source atom.[20] A combination of these two photoelectron diffraction techniques would therefore provide a very good method for studying ordered interfaces.

II. EXPERIMENTAL

The experiments were performed at the National Synchrotron Light Source at Brookhaven National Laboratory on beamline U3-C, a soft x-ray beamline with a five meter extended range grasshopper monochromator having a fixed exit geometry. The gold coated spherical grating (1200 $^{lines}/_{mm}$ and 3.7 m radius) covered the photon energy range 150 - 1000 eV. The energy resolution was $\Delta E \approx 3$ eV with 40 μm slits.

The data were collected in an ultra-high vacuum chamber ($P \leq 60$ nPa) which has been described previously.[21] The chamber was equipped with standard ultra-high vacuum surface science sample cleaning and preparation tools including a Varian LEED/Auger system, a Phi Ar^+ sputter gun, a UTI residual gas analyzer, and a home-built gas inlet system as well as a material evaporation source for overlayer preparation. The crystal was spotwelded between two tungsten wires onto a Vacuum Generators high-precision manipulator (x, y, z, θ, ϕ) equipped with liquid-nitrogen cooling; the crystal was cleaned by repetitive cycles of Ar^+ sputtering and subsequent annealing by electron bombardment from behind to 700 °C. The sample cleanliness was monitored using x-ray photoelectron spectroscopy (XPS) and checking for carbon (1s), nitrogen (1s), oxygen (1s), and sulfur (2p); no contamination was detected before or after the data collection which lasted 9.5 hours.

The photoemission spectra were collected using an angle-resolving electrostatic hemispherical electron energy analyzer (mean radius of 50 mm) which is rotatable 360° around the sample's vertical axis and 100° around the sample's horizontal axis. The analyzer pass energy was set to 160 eV and

the energy resolution was ~1.6 eV FWHM. The angular resolution of the double einzel input lens was ~±3°.

Synchrotron radiation is ≥98% linearly polarized. The angle of incidence of the light on the crystal was oriented 55° from the surface normal away from the crystal (011) plane. The photon polarization vector, $\vec{\varepsilon}$, was thus oriented 35° from the surface normal and perpendicular to the crystal (011) plane (see illustration in figure 2). The analyzer was oriented normal to the Ni(111) surface and the crystal was cooled to ~100 K throughout the data collection.

III. DATA COLLECTION

The raw data were a series of x-ray photoemission spectra; the photoelectron kinetic energy was scanned from 97 - 416 eV. The lower limit was chosen to avoid Ni 3*p* peak interference with the strong Ni *MNN* auger peak at 61 eV. The scan was terminated at the upper limit because the flux became too low to obtain high quality spectra. Using the de Broglie relation

$$k\left(\text{Å}^{-1}\right) = 0.5123\sqrt{E(\text{eV})} \qquad (1)$$

this photoelectron energy range corresponds to the magnitude of the photoelectron wave vector range 5.05 - 10.45 Å^{-1}. The spectra were recorded across this range in equal 0.10 Å^{-1} steps. Note that this is the wave vector as measured by the analyzer (*outside* of the crystal). The scattering calculations to be described later take place *inside* the crystal and were adjusted for the inner potential of the solid. Although the exact value of the

inner potential is unknown, it is ~10 eV for nickel; it was allowed to float during the modeling calculations.

Each photoemission spectrum was a 29.5 eV window encompassing the Ni $3p_{3/2}$ and Ni $3p_{1/2}$ peaks as well as two satellite peaks. These satellites were shifted from the Ni $3p_{3/2}$ by 5.5 eV and 12 eV to lower kinetic energy. Figure 1 is an example of one of these spectra and includes the fit for each of the four peaks. Each peak was fit with a Lorentzian convoluted with a Gaussian, a Voigt function, to model the natural linewidth and the experimental broadening, respectively. Each Voigt function was added to a Fermi step-function with a step-height scaled to the respective peak intensity and a step-width taken as the Gaussian width of the respective peak. In this way, the step-function models the inelastic scattering background of the photoemission spectrum. Summing each of the four Voigt functions and adding the inelastic background gave the total fit which is the solid line through the data points in figure 1.

IV. DATA REDUCTION AND ANALYSIS

The purpose of fitting the spectra is to extract the most accurate area from the peaks. This allows the data to be reduced to the $\chi(k)$ diffraction curve which contains the structural information. $\chi(k)$ is defined by[22]

$$\chi(k) = \frac{I(k)}{I_0(k)} - 1 \qquad (2)$$

where $I(k)$ is the peak area plotted as a function of the peak position in k-space. $I_0(k)$ is a smooth, slowly varying function with an oscillation frequency much lower than $I(k)$; $I_0(k)$ stems from the contribution of the

inelastic scattering processes and the varying atomic cross section. It is adequate to use a simple polynomial function of energy to fit $I_0(k)$.[23]

Removing $I_0(k)$ results in a removal from the FT the peaks $\lesssim 2$ Å. Note that this study is of the clean nickel surface and thus photoemission occurred from atoms several layers below the surface. Many forward scattering path-length differences from sub-surface emitting atoms will be on the order of $\lesssim 2$ Å. This forward scattering signal is therefore removed during the data reduction along with the standard $I_0(k)$. The resulting experimental ARPEFS $\chi(k)$ curve is thus dominated by backscattering.

The peak area was determined by integrating the Voigt functions over the spectrum window. The total experimental energy resolution was approximately 3.4 eV, obtained by quadratically summing the beamline resolution with the analyzer resolution. The spin-orbit splitting between the Ni $3p_{1/2}$ and Ni $3p_{3/2}$ photoelectron peaks was not well resolved and thus there was much intensity mixing between the respective Voigt functions during the fitting process. For this reason, the sum of these two peak areas was plotted against the k-position of the Ni $3p_{3/2}$ peak to finally plot the experimental $\chi(k)$ curve shown in figure 2 (solid line). The best-fit result from the multiple-scattering modeling calculations is also shown in figure 2 (dashed line) and will be discussed later.

A. Fourier Analysis

At this point, it is useful to study the auto-regressive linear prediction based Fourier transform (ARLP-FT) to move from momentum space to real space. In ARPEFS, the positions of the strong peaks in ARLP-FTs from adsorbate/substrate systems can be predicted with fairly good accuracy using

the single-scattering cluster (SSC) model together with the concept of strong backscattering from atoms located within a cone around 180° from the emission direction. The effective solid angle of this backscattering cone is ~30° - 60°; it is not unique, but is operationally defined simply by opening the angle until it can account for the observed FT peaks based on the crystal geometry. Signals from scattering atoms very close to the source atom may be observable even if the scatterers lie outside the nominal backscattering cone.

These FT peaks correspond to path-length differences (PLDs), ΔR_j, between the component of the photoemitted wave that propagates directly to the detector and the components which are first scattered by the atomic potentials within this backscattering cone.[6] Thus, the peak positions are

$$\Delta R_j = r_j\left(1-\cos\theta_j\right)+\phi_j \tag{3}$$

where r_j is the bond length, θ_j is the scattering angle (180° for exact backscattering), and ϕ_j is the atomic scattering phase shift. The scattering takes place inside the crystal and the ARPEFS data must be shifted from the measured $\chi\left(k_{\text{outside-crystal}}\right)$ to $\chi\left(k_{\text{inside-crystal}}\right)$ to account for the inner potential. In ARPEFS modeling calculations, the inner potential is treated as an adjustable parameter and is typically 5 - 15 eV. Thus, before Fourier transformation, the ARPEFS data presented here were shifted by 10 eV to higher kinetic energy.

The ARLP-FT of the experimental ARPEFS data is plotted in figure 3. Also illustrated in figure 3 is a schematic of the Ni(111) single crystal, assuming a bulk-terminated fcc surface, with a backscattering cone superimposed. The FT shows peaks due to scattering from atoms up to four

layers below the emitting atoms. The depth sensitivity of ARPEFS has been described previously and was found to be enhanced by multiple-scattering effects.[5]

The labeled atoms correspond to the labeled peaks in figure 3. Using the bulk nearest-neighbor spacing, 2.49 Å, and assuming a bulk-terminated surface, the expected peak positions can be calculated using simple geometry. These expected peak positions along with the actual peak positions and their corresponding shifts are listed in table 1. Also listed in table one is an assignment of the peak to single-scattering (SS) or double-scattering (DS) events. Additionally, the number of atoms contributing to each peak is listed in table 1.

The origins of the peaks labeled 2, 3, 4, 5, and 6 are straightforward. If a line is drawn from a surface emitter into the crystal and normal to the (111) plane, peaks 2, 3, and 6 occur due to single-scattering from the three atoms closest to this line in layers 2, 3, and 5, respectively. Nickel is fcc and thus peak 4 is due to direct backscattering (θ_j=180°) from the #4 atom which is in layer 4. Peak 5 is due to single-scattering from the six nearest neighbors to atom #4, the #5 atoms which are also in layer 4.

Peaks 2' and 3' may be attributed to atoms more laterally distant from the line described above. Peak 2' occurs due to single-scattering from the three second nearest-neighbors to this line in layer 2. Similarly, peak 3' occurs due to single-scattering from the three second nearest-neighbors to this line in layer 3.

Double-scattering may be detectable in the ARLP-FT as evidenced by peaks 2*, 3*, 4*, and 5*. The first event for peak 2*, for example, is scattering by the #2 atoms. The second event is scattering by the #2 atoms' six nearest neighbors. Given that there are three #2 atoms, eighteen atoms

are available for the second scattering event to give peak 2*. An analogous process holds for the 3* peak. Because there is only one #4 atom for each emitter in the fcc ($\dot{a}bc\dot{a}bc$) geometry, only six atoms are in position for the second scattering event to give peak 4*. However, there are six #5 atoms and thus thirty-six atoms for the second scattering event to give peak 5*.

These assignments due to double-scattering are somewhat speculative. It is believed that peaks 4* and 5* have a higher relative amplitude as compared to 2* and 3* because waves scattering in the fourth layer can be forward focused by atoms in the surface layer. Also, the higher probability for the second scattering event of peak 5* due to the greater number of atomic potentials will increase its relative amplitude.

A new result is also noted in this ARLP-FT. In addition to the backscattering peaks, the peak labeled 1 is due to single-scattering of the photoemitted wave from the six nearest neighbor atoms in the same (111) plane as the emitting atoms. This scattering path has not been observed previously for *s* initial state data or calculations because the photoemitted p_o wave destructively interferes with itself for the scattering angle θ_j=90° due to its negative parity. The photoemitted *d* and *s* waves which are interfering with themselves and with each other have positive parity; therefore, they do not cancel upon scattering from atoms in the same (111) plane as the emitting atoms. Thus, the frequency component labeled peak 1 is a physical part of the $\chi(k)$ diffraction curve and the appropriate PLD peak is observed. A peak that would be labeled 1' arising from scattering by the second nearest neighbors in the same layer as the emitting atoms would be seen at ~4.31 Å. If present, this weak feature is dominated by peak 2.

B. Multiple-Scattering Analysis

It has become standard to perform modeling calculations in an attempt to simulate the ARPEFS $\chi(k)$ curve. Using the single-scattering model of ARPEFS,[6,22] $\chi(k)$ can be written as

$$\chi(k) = \sum_j A_j(k) \cos\left[k\left(R_j - R_j \cos\theta_j\right) + \phi_j\right] \tag{4}$$

where $A_j(k)$ contains experimental geometry factors including the photon polarization direction and the electron emission direction as well as the scattering amplitude, aperture integration, and thermal averaging.

At $\theta_j = 0°$, there is zero path-length difference (PLD) between the direct and scattered photoelectron waves. Hence, interference between the direct and scattered photoelectron waves is detectable only through amplitude and phase differences, not by modulation of the signal. For forward scattering through angles close to 0°, the scattering amplitude is quite large, but many PLD values are correspondingly small and do not show up in the FTs. Experience with ARPEFS data indicates that PLDs $\lesssim 2$ Å will not show up in the FT analysis as discussed earlier. Modeling calculations are very useful because a variety of test cases can be used to better understand the scattering processes.

Typically, ARPEFS has been studied from an *s* initial state where the final state is a photoemitted p_0 wave. The multiple-scattering spherical-wave (MSSW) code developed by Barton and Shirley[6,22-24] has been proven accurate for *s* core-level photoemission.[6-11] However, the ARPEFS data and FTs from a *p* initial state require both *s* and *d* partial waves to describe the final state. A new code developed by Chen, Wu, and Shirley was used for

the calculations presented here.[25] This new code is based on the Rehr-Albers formalism.[26] Kaduwela and Fadley[27] developed a code based on this method which has been discussed and applied to photoelectron diffraction from arbitrary initial states by Friedman and Fadley.[28] This new code is sufficiently fast that fitting calculations can be performed for systems in which the photoemitters are in many layers and the core-level initial state has arbitrary angular momentum.

The radial dipole matrix elements, $R_{\ell_i \pm 1}$, and phase shifts, $\delta_{\ell_i \pm 1}$, were obtained from Goldberg, Fadley, and Kono[29] who developed them from Manson and Cooper's earlier work.[30] These values describe the shape and phase relationship between the two partial waves, $\ell_i \pm 1$, and thus the true $s+d$ final state as a function of the photoemitted electron kinetic energy.

To account for vibration effects of the bulk atoms, the mean square relative displacement (MSRD) was calculated using equation (33) by Sagurton *et al.*[4]

$$\left\langle u_i^2 \right\rangle \propto \frac{1}{M_i \theta_{\mathrm{D},i}} \left(1 + \frac{cT^2}{\theta_{\mathrm{D},i}^2} \cdots \right) \tag{5}$$

M_i is the atomic mass, $\theta_{\mathrm{D},i}$ is the correlated Debye temperature, T is the sample temperature, and c is a coefficient that varies slowly with temperature. For calculating the MSRD of the bulk Ni atoms, $\theta_{\mathrm{D},i}$ was 450 K and T was 80 K. Accounting for the surface atomic vibration has been discussed previously.[12,31]

The surface sensitivity of ARPEFS in the study of clean surfaces is strongly dependent on the inelastic mean free path (IMFP). Regarding modeling calculations, it is expected that the IMFP calculation is important

in obtaining a close fit to the data. Certainly, many emitters lie several layers below the surface region and their signal never escapes the crystal. The IMFP was included using the exponential damping factor $e^{-r/\lambda}$ where λ was calculated using the Tanuma, Powell, and Penn (TPP-2) formula.[18]

Powell[16] gives an overview of IMFP and attenuation length (AL) calculations and discusses the appropriate use of each. Powell also describes some of the problems and questions surrounding the IMFP and AL calculations. Application of IMFP calculations to x-ray photoelectron spectroscopy has been discussed by Jablonski and Powell.[17] Tanuma, Powell, and Penn[18] present a reasonable argument for using their TPP-2 formula to calculate the IMFP, λ (Å). They present the TPP-2 formula as

$$\lambda = \frac{E}{E_p^2\left[\beta \ln(\gamma E) - \frac{C}{E} + \frac{D}{E^2}\right]} \tag{6}$$

where E (eV) is the electron energy and E_p (eV) is the free electron plasmon energy as defined by

$$E_p = 28.8\left(\frac{N_v \rho}{M}\right)^{1/2} \tag{7}$$

N_v is the number of valence electrons per atom (or molecule), ρ $\left(g/cm\right)$ is the density, and M is the atomic (or molecular) weight. β, γ, C, and D are parameters defined as

$$\beta = -0.0216 + \frac{0.944}{\left(E_p^2 + E_g^2\right)^{1/2}} + 7.39 \times 10^{-4} \rho \tag{8}$$

$$\gamma = 0.191 \rho^{-0.50} \tag{9}$$

$$C = 1.97 - 0.91\left(\frac{N_v \rho}{M}\right) \tag{10}$$

$$D = 53.4 - 20.8\left(\frac{N_v \rho}{M}\right) \tag{11}$$

and E_g (eV) is the bandgap for non-conductors.

Figure 4 compares the TPP-2 formula for nickel and the $\lambda = ck$ formula where $c = 0.78$ Å^2 which has been used previously for ARPEFS modeling calculations.[32,33] The shape and magnitude for these IMFP curves are significantly different. However, also plotted in figure 4 is the $\lambda = ck$ formula for $c = 0.92$ Å^2 which adequately matches the TPP-2 formula for electron energies $\gtrsim$200 eV. Below 200 eV lies a significant amount of ARPEFS information and the effect of the different IMFP values is currently being studied.

Tanuma *et al.*[18] discuss why the TPP-2 formula is a good model and they also point out the causes of uncertainty. Angular anisotropies in the IMFP are another concern with respect to this study as well as with respect to fixed-energy, scanned angle photoelectron diffraction.[16] Certain crystallographic directions can enhance the depth sensitivity of ARPEFS due to forward focusing along a chain of atoms. It is not yet known how the angular anisotropies will affect the shape or magnitude of the curves shown in figure 4. It is certainly a more complicated problem to calculate a physically accurate signal loss due to inelastic scattering as a function of E, θ, and ϕ for a given sample and crystallographic surface.

The analyzer acceptance angle as well as the emission and polarization directions and were set to match the experiment as described earlier. The atomic-scattering phase shifts were calculated in situ by using the atomic potentials tabulated by Moruzzi *et al.*[34] Figure 2 plots the best fit

(dashed line) on top of the experimental ARPEFS data (solid line). For this fit, a 74 atom cluster was used and the inner potential was optimized at 9.8 eV. The spacing between the first two nickel layers was determined to be 2.06(1) Å -- a +1.5% expansion of the bulk value, 2.03 Å. By contrast, for clean Cu(111), LEED studies have detected a surface *contraction* of ~0.7% from the bulk value, 2.09 Å.[35,36]

C. Discussion of Error

The best fit is determined by an R-factor minimization. A three-step fitting process is used to determine the true R-factor minimum to prevent convergence to a local minimum. The initial coarse-fitting minimizes the $\tilde{R}$-factor, $\tilde{R} = R_a$ where

$$R_a = \frac{\sum_i \left[\chi_{i,c}(k) - \chi_{i,e}(k)\right]^2}{\frac{1}{2}\sum_i \left[\chi_{i,c}^2(k) + \chi_{i,e}^2(k)\right]} \tag{12}$$

using a simple net search.[25] $\chi_{i,c}(k)$ and $\chi_{i,e}(k)$ are the points in the calculated and experimental $\chi(k)$ curves respectively. Second, the code again minimizes $\tilde{R} = R_a$ using the Downhill Simplex Method in Multidimensions.[37] Finally, the code minimizes $\tilde{R} = R$ where

$$R = \frac{\sum_i \left[\chi_{i,c}(k) - \chi_{i,e}(k)\right]^2}{\sum_i \chi_{i,e}^2(k)} \tag{13}$$

using the Nonlinear Marquardt Method.[37]

While fitting, the largest effects stem from changes in the inner potential and the interlayer spacing between the first two Ni layers. Figure 5 shows a contour plot of the R-factor as the inner potential and Ni_1-Ni_2 interlayer spacing are varied. Even with an uncertainty of ±2.6 eV in the inner potential, the precision of ARPEFS is ±0.01 Å.

V. Ni 3*p* DATA COMPARED WITH $\sqrt{3}\times\sqrt{3}R30°$Cl/Ni(111) DATA

Figure 6 compares the Ni 3p data with $\sqrt{3}\times\sqrt{3}R30°$Cl/Ni(111) data published previously.[19] This comparison illustrates the differences and similarities between the s and the p core-level initial state ARPEFS data. The ARPEFS $\chi(k)$ curves are roughly 180° out of phase. This final-state effect is expected and has been seen previously.[13-15] Also, the FTs are remarkably similar, with ARLP-FT peaks for backscattering from layers below the source atom being resolved in both cases. There is a slight shift in lattice spacing between the two samples which is evident in the FT. Additionally, the Ni 3p data FT show a peak at ~2.5 Å due to effects described above whereas the Cl 1s data FT has no such peak.

The similarity of the two ARLP-FT spectra shows that ARPEFS of a clean crystal is dominated by backscattering. The ARPEFS intensity can be regarded as arising from the sum of contributions from source atoms in each layer as if it were the surface layer. If we neglect forward scattering from atoms in layers above the source atoms, the ARPEFS intensity is modulated due to backscattering from the atoms in layers below the source atoms. Due to the finite mean free path, the signal from the sub-surface layer atoms is damped.

VI. CONCLUSION

The first non-*s* initial state ARPEFS study of a clean surface for the purpose of further understanding the technique is reported. The clean surface ARPEFS data resemble data for adsorbate systems, showing strong backscattering signals from atoms up to four layers *below* the source atoms. In addition to the backscattering, the Ni 3*p* data show a peak in the FT at ~2.5 Å corresponding to scattering from the six nearest neighbor atoms in the same crystal layer as the emitting atoms. This result is forbidden by symmetry for *s* initial state photoemission scattering from a point source but is expected from *p* initial state photoemission. Evidence was also seen for single-scattering events from atoms laterally distant from the emitting atom as well as double-scattering events.

An adsorbate system, $\sqrt{3} \times \sqrt{3}R30°$Cl/Ni(111),[19] was compared with the clean Ni 3*p* data. Although this previously published data was photoemission taken from the Cl 1*s* core level, the data and FTs from *s* versus *p* initial states agree such that the backscattering cone model is supported by this work.

It has been shown that photoelectron holography signals from clean surfaces are dominated by forward scattering, with atomic positions being imaged up to three layers *ahead* of the source atom.[20] A combination of these two photoelectron diffraction techniques would therefore provide a very good method for studying ordered interfaces.

ACKNOWLEDGMENTS

Much appreciation is expressed to Ajith Kaduwela for helpful discussions regarding PEH as well as his scattering code. This work was supported by the Director, Office of Energy Research, Office of Basic Energy Sciences, Chemical Sciences Division of the U.S. Department of Energy under Contract No. DE-AC03-76SF00098. The experiments were performed at the National Synchrotron Light Source at Brookhaven National Laboratory which is supported by the U. S. Department of Energy's Office of Basic Energy Sciences.

TABLES

- Table 1: Scattering paths with the calculated PLD (based on 2.49 Å nearest neighbor spacing) along with the actual peak positions and the respective shifts. Layer 1 is defined as the same layer as the emitting atom.

Peak Number	Calculated PLD (Å)	Peak Position (Å)	Peak Shift (Å)	Scattering	# of Atoms Contributing
1	2.49	2.36	-0.13	SS	6
2	4.52	4.69	0.17	SS	3
2'	5.55	5.99	0.44	SS	3
2*	7.01	7.60	0.59	DS	3 × 6
3	8.37	8.45	0.08	SS	3
3'	9.04	9.07	0.03	SS	3
3*	10.86	10.18	-0.68	DS	3 × 6
4	12.18	12.51	0.33	SS	1
5	12.67	12.90	0.23	SS	6
4*	14.67	14.68	0.01	DS	1 × 6
5*	15.16	15.09	-0.07	DS	6 × 6
6	16.37	16.00	-0.37	SS	3

FIGURES

- Figure 1: Example photoemission spectrum showing the data as well as the four Voigt functions and the step function used to fit the data.

- Figure 2: Normal emission Ni(111) $3p$ ARPEFS $\chi(k)$ data (solid line) and best fit (dashed line). A schematic of the experimental geometry is shown.

- Figure 3: ARLP based FT of the Ni $3p$ ARPEFS data. A model of the lattice with the backscattering cone indicates the scattering atoms corresponding to the FT peaks.

- Figure 4: Calculation of the IMFP as proposed in the previous ARPEFS studies involving Ni using $\lambda = ck$ and $c = 0.78$ Å^2. Also plotted is a calculation for $c = 0.92$ Å^2 which better approximates the TPP-2 result (dashed line) for electron energies >200 eV.

- Figure 5: Contour plot showing how the R-factor varies with the Ni_1-Ni_2 interlayer spacing and the inner potential. Even with an uncertainty of ±2.6 eV in the inner potential, the precision of ARPEFS is ±0.01 Å.

- Figure 6: The top panel overlays the $\sqrt{3} \times \sqrt{3}R30°$Cl/Ni(111) (dashed line) with the Ni $3p$ (solid line) experimental ARPEFS curves. The bottom panel overlays their respective ARLP-based FTs.

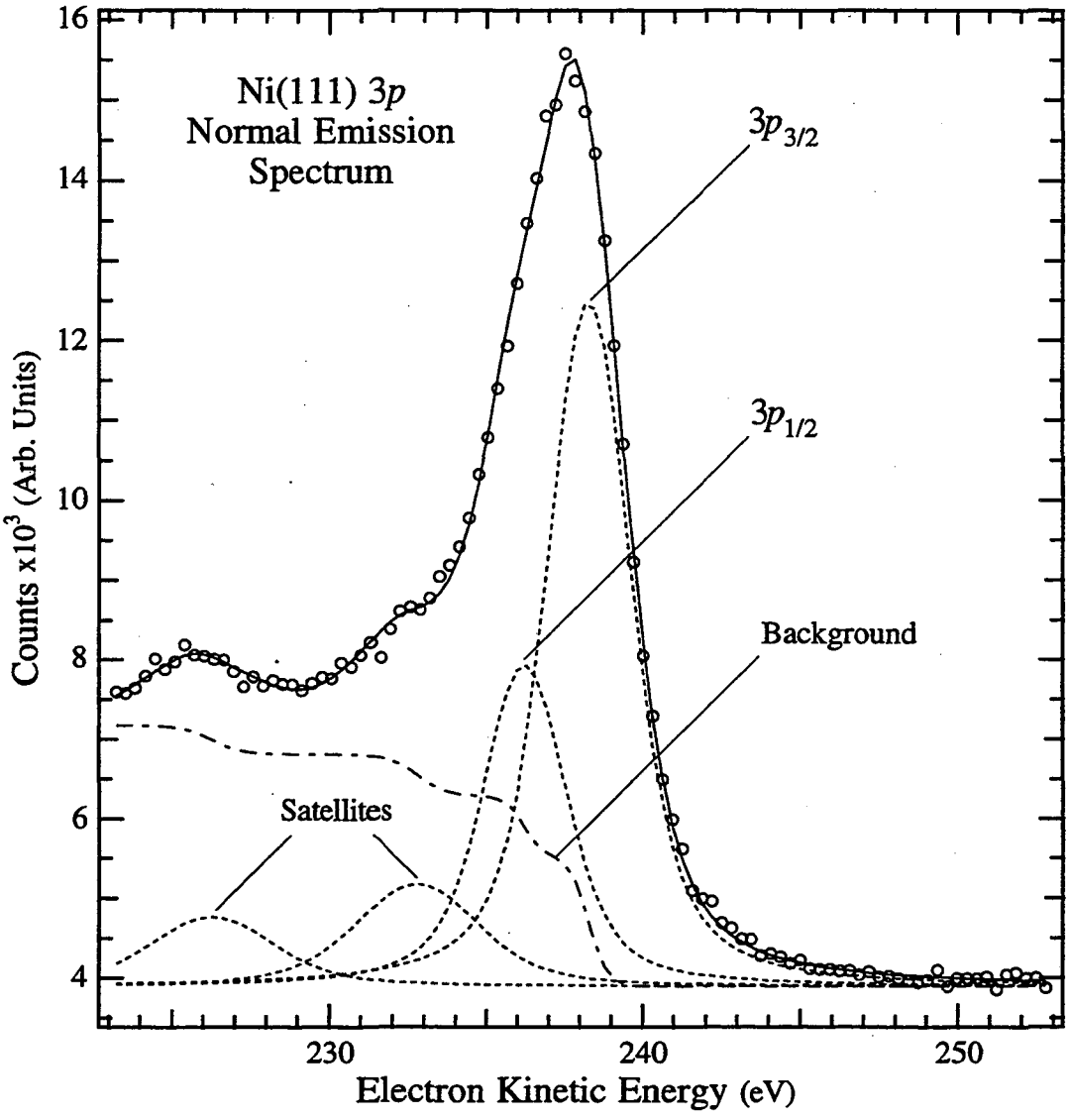
Ni(111) 3p
Normal Emission
Spectrum
3p3/2
3p1/2
Background
Satellites
Counts x10^3 (Arb. Units)
Electron Kinetic Energy (eV)
16
14
12
10
8
6
4
230
240
250

Figure 1

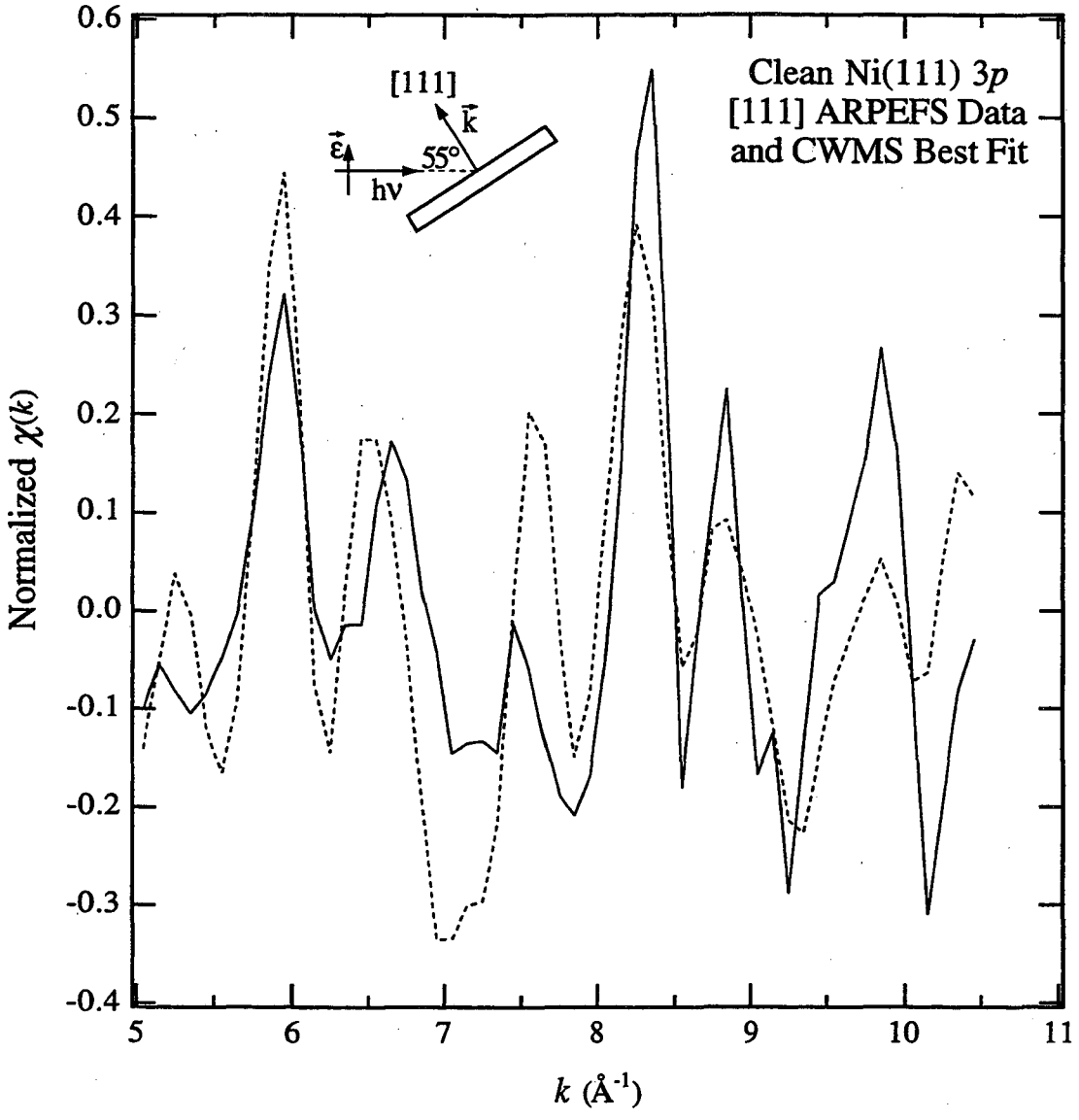
Clean Ni(111) 3p
[111] ARPEFS Data
and CWMS Best Fit
[111]
k
ε
55°
hν
Normalized χ(k)
k (Å-1)
0.6
0.5
0.4
0.3
0.2
0.1
0.0
-0.1
-0.2
-0.3
-0.4
5
6
7
8
9
10
11

Figure 2

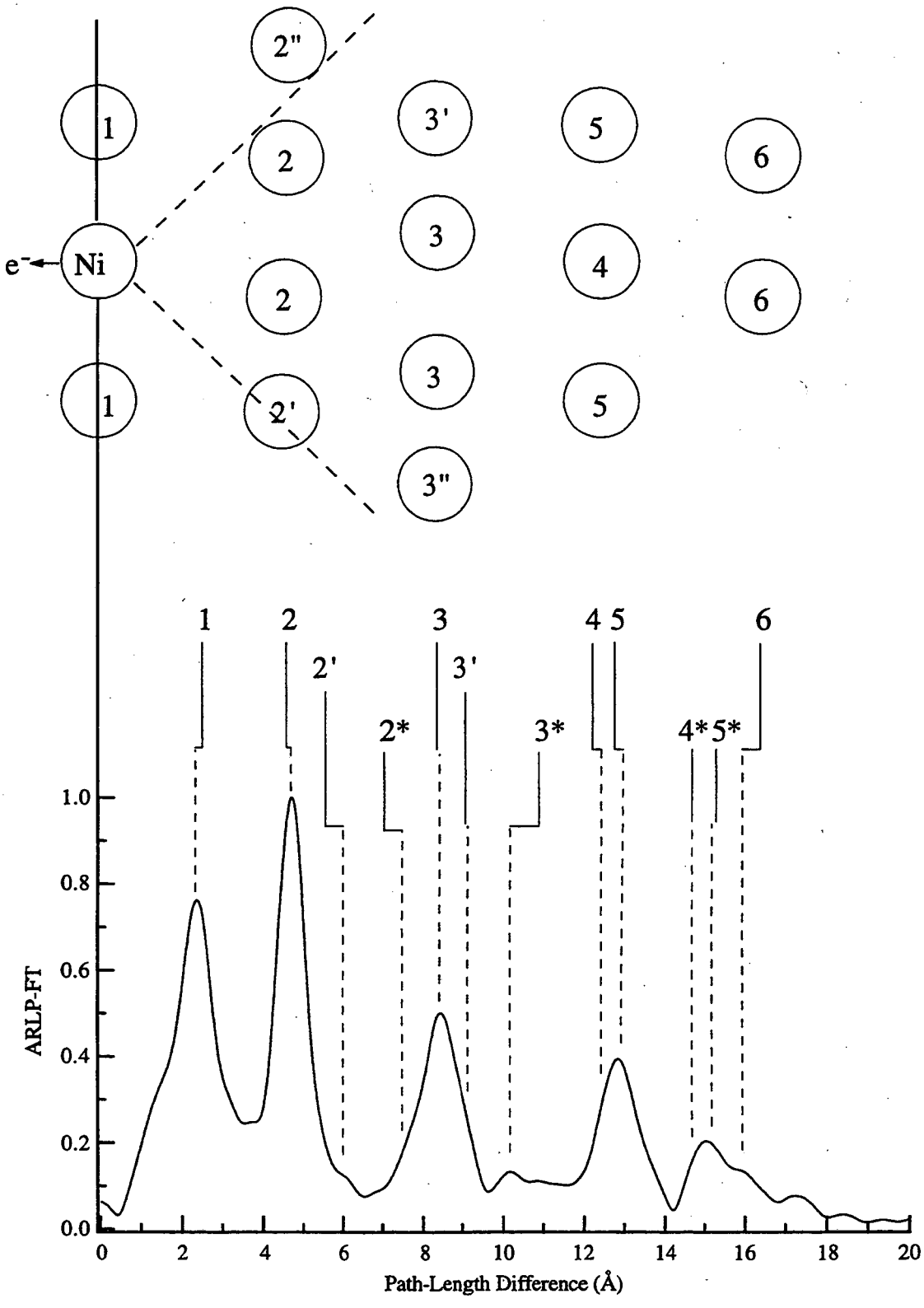
2"
1
2
3'
5
6
e⁻
Ni
2
3
4
6
1
2'
3
5
3"
1
2
3
4 5
6
2'
3'
2*
3*
4* 5*
1.0
0.8
0.6
0.4
0.2
0.0
ARLP-FT
0
2
4
6
8
10
12
14
16
18
20
Path-Length Difference (Å)

Figure 3

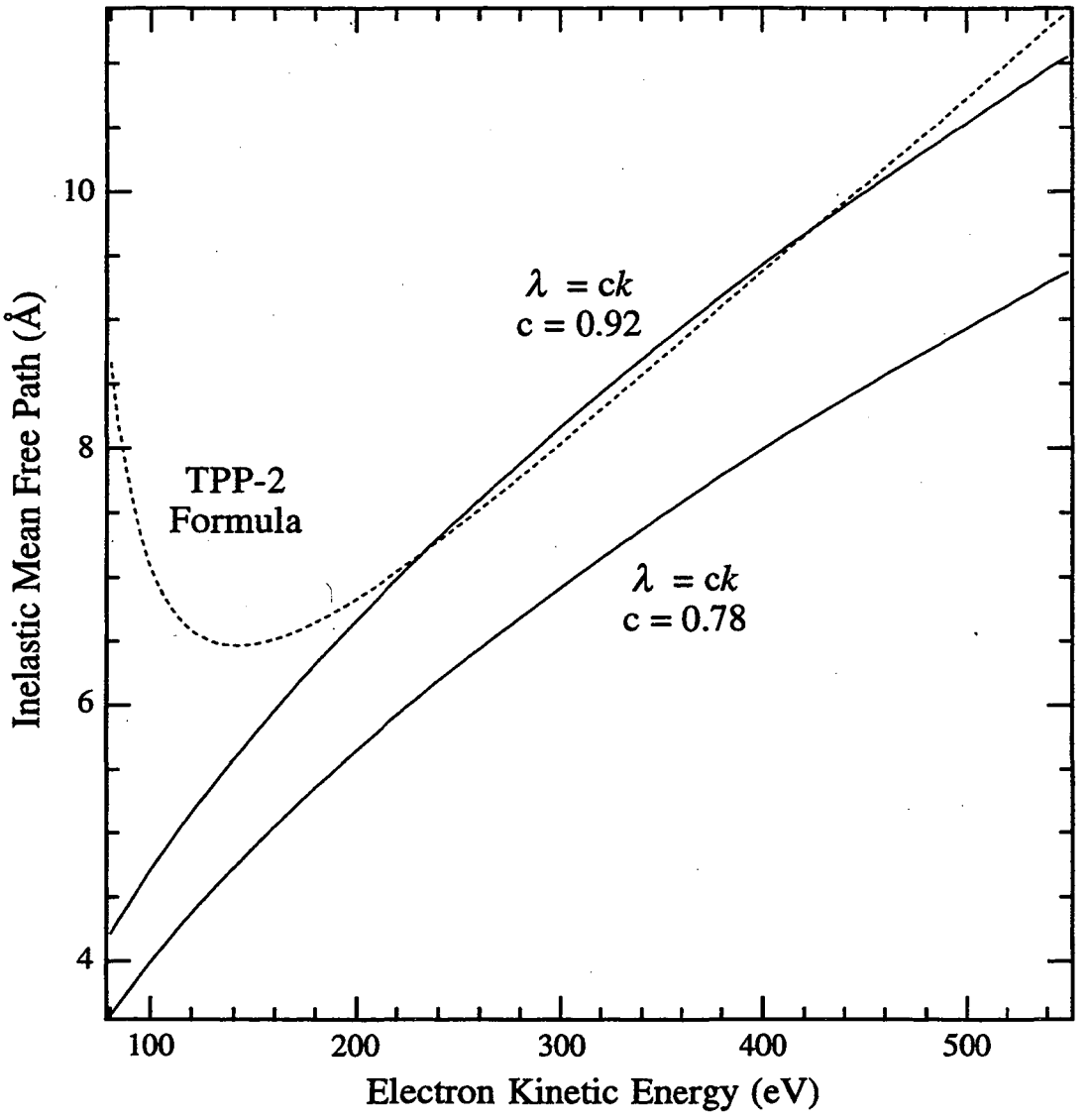
Inelastic Mean Free Path (Å)
10
8
6
4
100
200
300
400
500
Electron Kinetic Energy (eV)
λ = ck
c = 0.92
TPP-2
Formula
λ = ck
c = 0.78

Figure 4

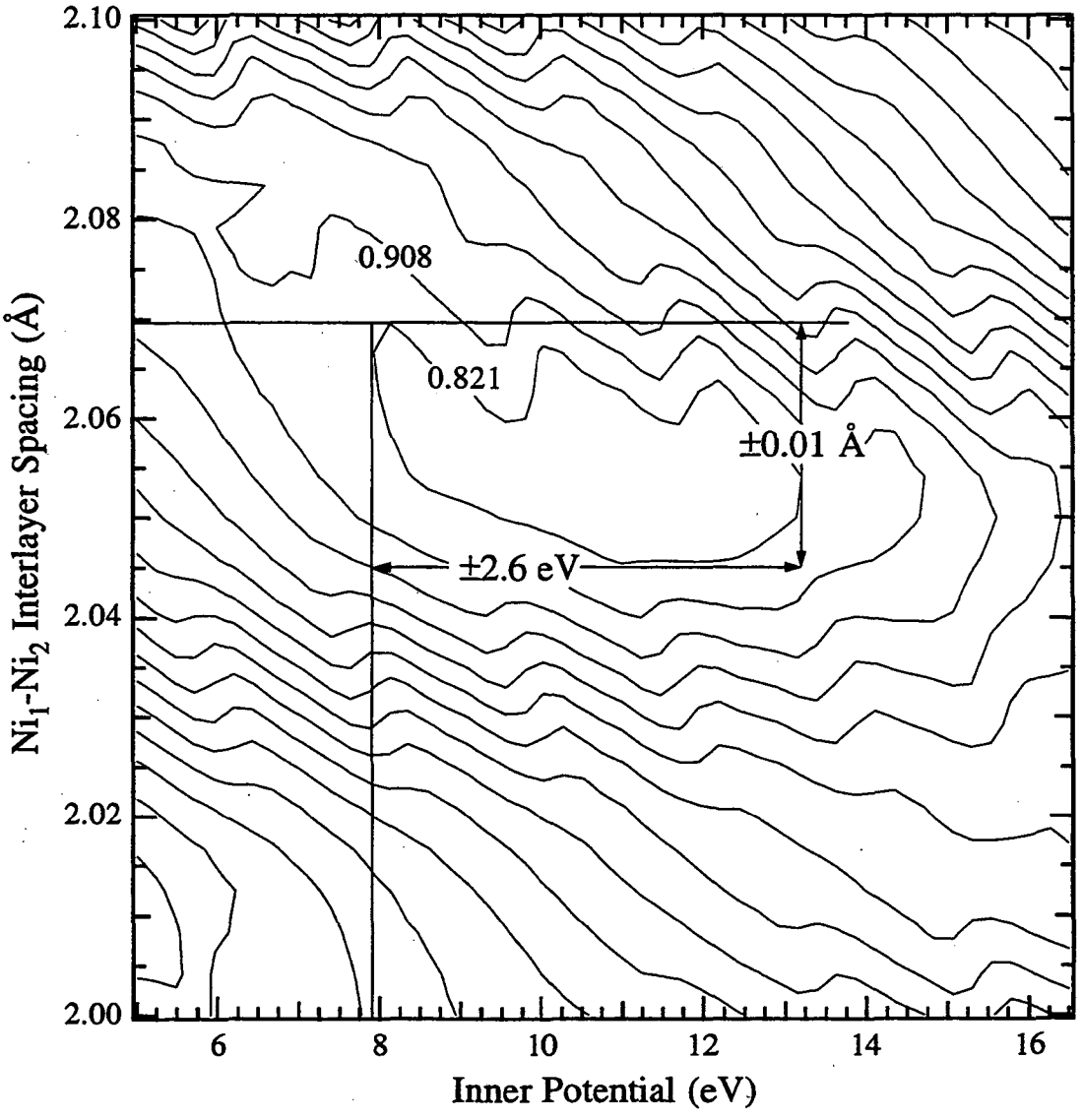
2.10
2.08
2.06
2.04
2.02
2.00
0.908
0.821
±0.01 Å
±2.6 eV
6
8
10
12
14
16
Ni1-Ni2 Interlayer Spacing (Å)
Inner Potential (eV)

Figure 5

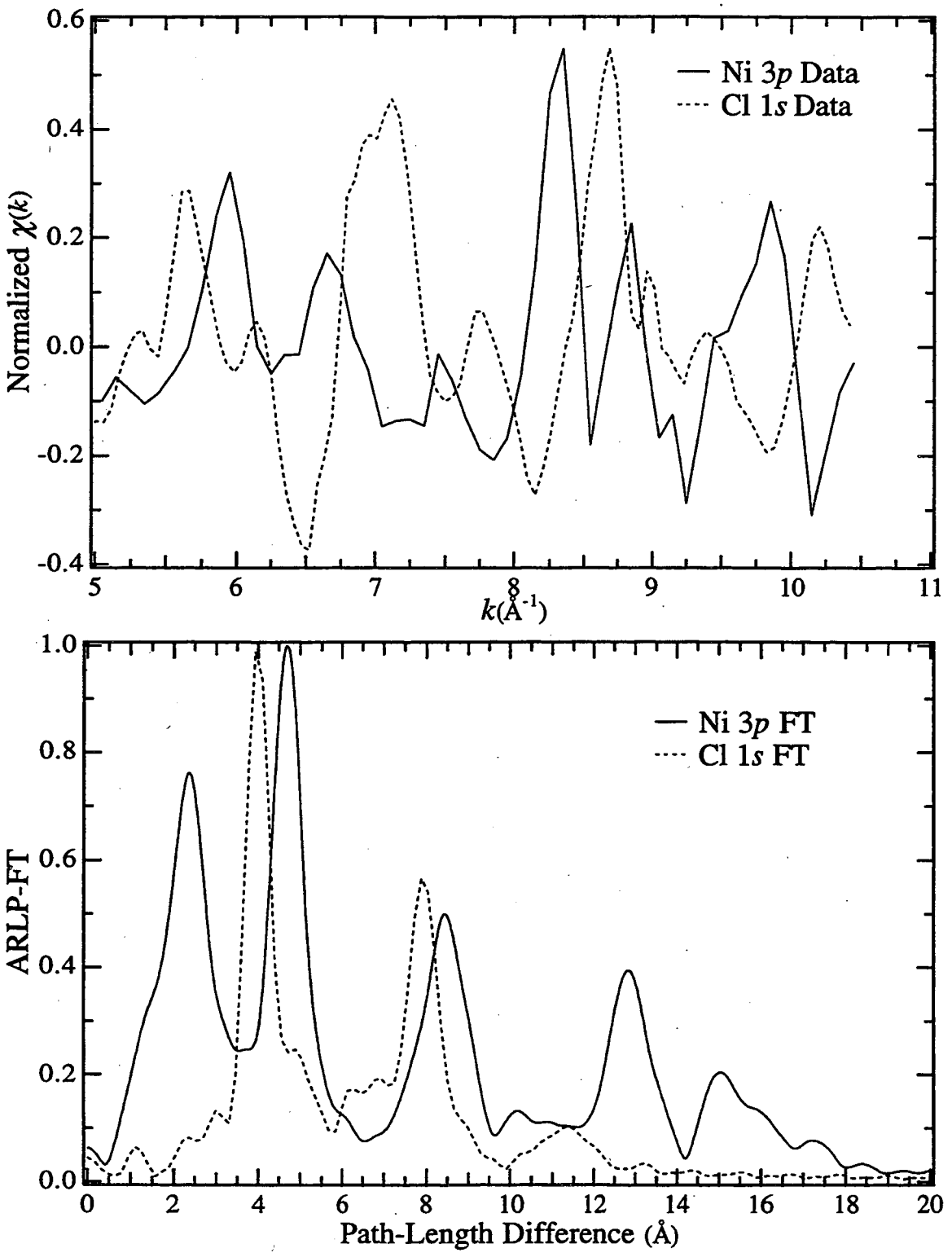
Ni 3p Data
Cl 1s Data
Normalized χ(k)
k(Å-1)
Ni 3p FT
Cl 1s FT
ARLP-FT
Path-Length Difference (Å)

Figure 6

REFERENCES

[1]S.D. Kevan, D.H. Rosenblatt, D. Denley, B.C. Lu and D.A. Shirley, Phys. Rev. Lett. **41**, 1565(1978).

[2]J.J. Barton, C.C. Bahr, Z. Hussain, S.W. Robey, J.G. Tobin, L.E. Klebanoff and D.A. Shirley, Phys. Rev. Lett. **51**, 272(1983).

[3]D.P. Woodruff, D. Norman, B.W. Holland, N.V. Smith, H.H. Farrell and M.M. Traum, Phys. Rev. Lett. **41**, 1130(1978).

[4]M. Sagurton, E.L. Bullock and C.S. Fadley, Surf. Sci. **182**, 287(1987).

[5]Y. Zheng and D.A. Shirley, Chem. Phys. Lett. **203**, 114(1993).

[6]J.J. Barton, C.C. Bahr, S.W. Robey, Z. Hussain, E. Umbach and D.A. Shirley, Phys. Rev. B **34**, 3807(1986).

[7]S.W. Robey, C.C. Bahr, Z. Hussain, J.J. Barton, K.T. Leung, J.R. Lou, A.E. Schach von Wittenau and D.A. Shirley, Phys. Rev. B **35**, 5657(1987).

[8]L.Q. Wang, A.E. Schach von Wittenau, Z.G. Ji, L.S. Wang, Z.Q. Huang and D.A. Shirley, Phys. Rev. B **44**, 1292(1991).

[9]Z.Q. Huang, L.Q. Wang, A.E. Schach von Wittenau, Z. Hussain and D.A. Shirley, Phys. Rev. B **47**, 13626(1993).

[10]Z.Q. Huang, Z. Hussain, W.T. Huff, E.J. Moler and D.A. Shirley, Phys. Rev. B **48**, 1696(1993).

[11]Y. Zheng, E. Moler, E. Hudson, Z. Hussain and D.A. Shirley, Phys. Rev. B **48**, 4960(1993).

[12]W.R.A. Huff, Y. Chen, X.S. Zhang, L.J. Terminello, F.M. Tao, Y.K. Pan, S.A. Kellar, E.J. Moler, Z. Hussain, H. Wu, Y. Zheng, X. Zhou, A.E. Schach von Wittenau, S. Kim, Z.Q. Huang, Z.Z. Yang and D.A. Shirley, (to be published).

[13]W.R.A. Huff, Y. Zheng, Z. Hussain and D.A. Shirley, J. Phys. Chem. **98**, 9182(1994).

[14]S.Y. Tong and J.C. Tang, Phys. Rev. B **25**, 6526(1982).

[15]J.C. Tang, Chin. Phys. Lett. **4**, 321(1987).

[16]C.J. Powell, J. Electron Spectrosc. Relat. Phenom. **47**, 197(1988).

[17]A. Jablonski and C.J. Powell, Surf. Interface Anal. **20**, 771(1993).

[18]S. Tanuma, C.J. Powell and D.R. Penn, Surf. Interface Anal. **20**, 77(1993).

[19]L.-Q. Wang, Z. Hussain, Z.Q. Huang, A.E. Schach von Wittenau, D.W. Lindle and D.A. Shirley, Phys. Rev. B **44**, 13711(1991).

[20]B.L. Petersen, L.J. Terminello, J.J. Barton and D.A. Shirley, Chem. Phys. Lett. **213**, 412(1993).

[21]S.D. Kevan, *Ph.D. Thesis*, The University of California, Berkeley, LBL-11017(1980).

[22]J.J. Barton, S.W. Robey and D.A. Shirley, Phys. Rev. B **34**, 778(1986).
[23]J.J. Barton, *Ph.D. Thesis*, The University of California, Berkeley, LBL-19215(1985).
[24]J.J. Barton and D.A. Shirley, Phys. Rev. B **32**, 1892(1985).
[25]Y. Chen, H. Wu and D.A. Shirley, *CWMS Code - Unpublished*, (1995).
[26]J.J. Rehr and R.C. Albers, Phys. Rev. B **41**, 8139(1990).
[27]A. Kaduwela, *Ph.D. Thesis*, University of Hawaii at Manoa, Honolulu, (1991).
[28]D.J. Friedman and C.S. Fadley, J. Electron Spectrosc. Relat. Phenom. **51**, 689(1990).
[29]S.M. Goldberg, C.S. Fadley and S. Kono, J. Electron Spectrosc. Relat. Phenom. **21**, 285(1981).
[30]S.T. Manson and J.W. Cooper, Phys. Rev. **165**, 126(1968).
[31]R.E. Allen, G.P. Alldredge and F.W. de Wette, J. Chem. Phys. **54**, 2605(1971).
[32]S.W. Robey, J.J. Barton, C.C. Bahr, G. Liu and D.A. Shirley, Phys. Rev. B **35**, 1108(1987).
[33]M.P. Seah and W.A. Dench, Surf. Interface Anal. **1**, 1(1979).
[34]V.L. Moruzzi, J.F. Janak and A.R. Williams, *Calculated Electronic Properties of Metals*, (Pergamon Press, Inc., New York, 1978).
[35]S.P. Tear, K. Roll and M. Prutton, J. Phys. C **14**, 3297(1981).
[36]S.A. Lindgren, L. Wallden, J. Rundgren and P. Westrin, Phys. Rev. B **29**, 576(1984).
[37]W.H. Press, S.A. Teukolsky, W.T. Vetterling and B.P. Flannery, *Numerical Recipes in Fortran: The Art of Scientific Computing*, 2 ed., (University Press, Cambridge, 1992).

LAWRENCE BERKELEY NATIONAL LABORATORY
UNIVERSITY OF CALIFORNIA
TECHNICAL & ELECTRONIC INFORMATION DEPARTMENT
BERKELEY, CALIFORNIA 94720